Int. J. Nano Dimens., 15 (1): 35-48, Winter 2024

ORIGINAL ARTICLE

Numerical investigation of mixed convection in a porous lid-driven cavity filled with kerosene-Al_2O_3 nanofluid

Najmeh Hajialigol

Mechanical Engineering Department, Hamedan University of Technology, 65155-579 Hamedan, Iran

Received 11 October 2023, revised 05 November 2023, accepted 06 November 2023, available online 09 November 2023

Abstract

This research deals with the numerical analysis of the heat transfer characteristics of the unsteady combination of alumina-kerosene nanofluid enclosed in a porous cavity with a moving lid. The governing equations of fluid flow and conjugate heat transfer along with the relevant boundary conditions are applied to express the physical problem mathematically. First, the boundary conditions and governing equations are converted into non-dimensional forms by suitable transformation series. In the next step, the finite element method based on Galerkin residue was used to solve the transformed non-dimensional equations. The evaluation is shown by previous studies and found to be excellent in resolution. Numerical solutions are obtained in a wide range of governing variables. In this study, Solid volume fraction (φ), Richardson number (Ri), Reynolds number (Re), etc. are the governing variables. The numerical results of thermal fields and flow are graphically shown according to the average Nusselt number, streamlines, and isotherms on the cavity's hot surface. It is found that Ri has a wide influence on the streamlines and isotherms in the cavity as well as in specifying the average rate of heat transfer.

Keywords: *Finite Element Method; Heat Transfer; Mixed Convection; Nanofluid; Porous Lid-Driven Cavity.*

How to cite this article

Hajialigol N., Numerical investigation of mixed convection in a porous lid-driven cavity filled with kerosene-Al_2O_3 nanofluid. Int. J. Nano Dimens., 2024; 15(1): 35-48.

INTRODUCTION

There are many engineering applications for heat transfer, including solar collectors, heat exchangers, nuclear reactors, air conditioners, electrical and micro-electrics equipment, automobiles, aircraft, refrigeration, etc., where heat is continuously produced during the relevant processes. Excessive heat amounts can harm these devices; therefore, the extra heat must be quickly dissipated to the surrounding environment using a mechanism of heat transfer. To this end, engineers and researchers around the world are conducting studies on convective heat transfer to achieve effective fluid with advanced thermophysical features. Their research has found a new motivation with the nanofluid invention. Nanofluids are also used to produce better lubricants and oils, for medical targets, etc. Choi and Eastman [1] introduced the nanofluid which has higher thermal conductivity than conventional fluids and is usually consists of solid nanoparticles and liquid base. Buongiorno [2] presented a complete model of nanofluid convective heat transfer considering Brownian diffusion and thermophoresis as crucial mechanisms in nanofluids. Kakaç and Pramuanjaroenkij [3] reviewed the experimental and theoretical research on the increase of the interface between the solid and liquid surface, different thermal conductivity and viscosity models in a porous media and the improvement of the heat transfer rate of nanofluids. Sajid and Ali [4] reviewed the use of nanofluids for cooling different categories of thermal devices. Alhajaj *et al.* [5] performed the best differential analysis of nanofluid configuration for heat recovery. The heat transfer rate for different types of nanofluids in a multi-pipe heat exchanger was experimentally calculated by Manzoor and Saghir [6]. They found that the maximum rate of heat extraction could be

* Corresponding Author Email: *n.hajialigol@hut.ac.ir*

1% vol water/TiO_2 nanofluid.

Heat transfer efficiency of nanofluid in heat exchangers with various shapes was summarized by Olabi *et al.* [7]. Another significant method of increasing the rate of heat transfer is the usage of porous media. The interface between the liquid and solid surfaces in a porous medium, have been increases and leads to the development of the heat transfer rate. Nield and Bejan [8] detailed the convection within the porous media. Several researchers investigated the convection heat transfer inside a porous media with nanofluids in porous surfaces and various enclosure shapes. Zing *et al.* [9] investigated a porous media with a water-based nanofluid with two annealed pyrolytic graphite and copper nanoparticles in a heat exchanger. Their outcomes displayed that the highly conductive porous media can lead to better cooling efficiency. Xu *et al.* [10] reviewed the metal porous foam applications such as heat transfer of nanofluid. Alhajaj *et al.* [11] used two experimental and numerical methods to increase heat transfer within a porous passage along with hybrid fluid and nanofluid.

Sheremet and Pop [12] examined the natural convection within a porous cylindrical horizontal cavity. They considered the Darcy-Boussinesq approximation for nanofluid and porous media. Gros *et al.* [13] numerically studied nanofluid flow caused by buoyancy and heat transfer inside a metal foam or square cavity filled with glass beads. Yahya and Saghir [14] determined the rate of heat removal in a circular tube and flat pipe heat exchanger by including a porous media and nanofluid. They found that for the heat removal process, a flat pipe heat exchanger is more efficient compared to a circular tube. Karim *et al.* [15] performed a numerical simulation for the flow inside a long permeable cavity with two semi-cooled walls. Plant and Saghir [16] investigated a heat exchanger filled with porous medium with alumina nanofluid to achieve the optimal heat transfer rate. Aly *et al.* [17] studied the nanofluid natural convection flow in a heterogeneous homogeneous and porous media in a newly shaped cavity. Izadi *et al.* [18] investigated the hybrid nanofluid heat transfer in a porous cavity that is subjected to Lorentz, buoyancy, and Kelvin forces, taking into account variable porosity analytically. Several researchers have investigated the convective heat transfer in the Lorentz force presence for various complex cavity shapes, such as a permeable medium modelled by Darcy's law which has been demonstrated by CVFEM simulation, Rayleigh number, the impact of nanofluid volume fraction, and Hartmann number on streamlines and isotherms [19-21].

Xu *et al.* [22] analyzed the nanofluid flow in a channel filled with metal porous foam and forced convective heat transfer. They found that there must be a local thermal non-equilibrium phenomenon with a large difference in the solid and fluid thermal conductivity. Al-Weheibi *et al.* [23] buoyancy and flow-based heat transfer for different porosity and permeability considering thermal non-equilibrium between the nanofluid and the permeable media. They stated that for flow in a porous media, the Nu_{avg} is higher with variable porosity compared to constant porosity. Kalbani *et al.* [24] investigated the entropy production by nanofluid inside a tilted square cavity with magnetic flux. They concluded that friction is the most important factor in entropy generation and that the bottom heated wall generated maximum entropy.

Mixed convection is a combination of forced and natural convection and has many feasible applications including electronic cooling, nuclear reactors, lubrication technology, food processing, geothermal application, etc. Therefore, the attention of many researchers has been drawn to the nanofluids mixed convection heat transfer inside porous media. Entropy production and mixed convection inside a porous tilted open channel such as a cavity saturated with nanofluid was numerically were investigated by Hussain *et al.* [25]. The findings displayed that to attain the maximum heat transfer rate, 135º is the optimal inclination angle for the inclined channel. The steady mixed convective flow along an inclined channel filled by a porous media was investigated by Cimpean and Pop [26] and analytical results were presented for three various nanofluids. They also studied the parameters in the number of pellets in the channel inclination angle, flow mixed convection, and a specific nanoparticle solid-volume fraction.

The steady laminar mixed convective flow and water-copper nanofluid heat transfer inside a trapezoidal porous enclosure with various trapezoidal sidewall angles, Darcy and Reynolds numbers and nanoparticle volume fraction were examined by Al-Rashed *et al.* [27]. The outcomes exhibited that local Nusselt number

and fluid velocity decreases with a decrease of Darcy number. The effects of the rotating cooler and heater located in a porous square chamber on the mixed convection flow of nanofluid with various Rayleigh numbers, the cooler and heater rotation directions and Ri numbers were simulated by Tahmasbi *et al.* [28]. Also, they optimized the size of the pore inside the porous medium to obtain the maximum Nusselt value using a pattern search optimization algorithm. Selimefendigil and Chamkha [29] investigated the magnetohydrodynamic hybrid nanofluid mixed convection in a divided square cavity containing a porous layer with a triangular form. They stated that the inclination angle of the porous media and the strength of the magnetic field have a significant effect on the rate of heat transfer. Rajarathinam *et al.* [30] conducted a parametric study on the unsteady mixed convective heat transfer growth inside a fluid-filled porous rectangular cavity inclined through three various kinds of moving lids for different parameters including nanoparticle solid volume fraction, cavity inclination angle, and Darcy and Richardson numbers. Taking into account the model of Hazen-Dupain-Darcy, mixed convection inside a cavity with sloshing porosity for porous media was analyzed by Ahmad and Ali [31]. Transient nanofluid (alumina-water) mixed convection inside a two-layer cavity with a movable lid and various thermal properties, porosity, and permeability were studied by Astanina *et al.* [32].

Investigations show that there are few studies on the convection of an unstable mixture of saturated nanofluids inside a porous media. In this study, the convective flow of an unsteady mixture inside a porous medium through a saturated cavity with a movable lid is considered. Also, the current study numerically evaluated the impact of heating location on mixed convection in enclosures with movable lids filled with alumina-kerosene nanofluid. This research focused on studying of the influences of nanoparticle concentration, size-dependent thermal conductivity, and temperature on mixed convection of several relevant parameters, including heat source location, lid motion direction, Richardson number and particle volume fraction on the mixed convection characteristics inside the enclosure.

MATERIALS AND METHODS

The porous square enclosure with a movable lid filled with Al_2O_3-kerosene nanofluid is shown in Fig. 1. The cavity height and width are indicated by L. The cavity right wall is kept at a cold temperature T_c, while a heat source (with T_h) and length L/3 are placed on the left wall. The remaining parts of the left wall and the cavity's upper and lower horizontal walls are insulated. Two various cases (cases I (Fig. 1a) and II (Fig. 1b)) are taken into account in Fig. 1. The upper wall is moves to the right and left at the same velocity in case I and case II, respectively.

The nanofluid is taken into account as laminar in the enclosure, incompressible and Newtonian. It is assumed that the nanoparticles are homogeneous in terms of shape and size. In this study, nanoparticles are taken into account spherical with a diameter of 40 nm. It is assumed that no slip happens between alumina nanoparticles and kerosene and they are in thermal equilibrium. Table 1 shows the features of nanofluids. The porous bed must be saturated,

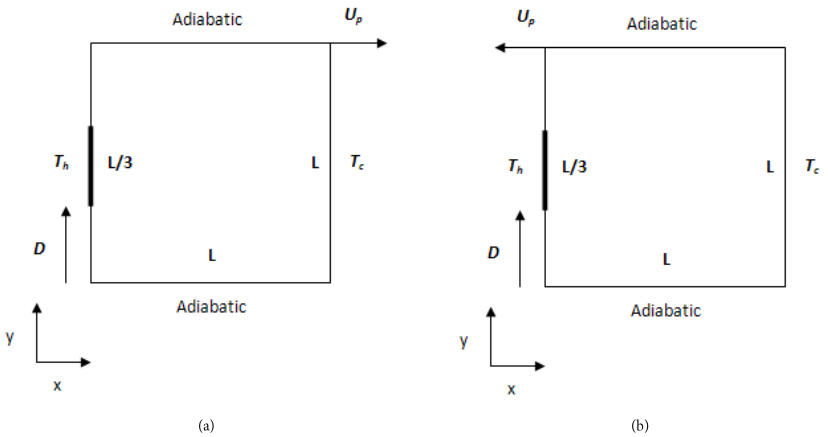

Fig. 1. Physical model and coordinates for two cases: (a) Case I; (b) Case II.

Table 1: Thermophysical characteristics of Al_2O_3 nanoparticles and kerosene (Mahmoodi and Kandelousi [33]).

Property	Fluid phase (Kerosene)	Al2O3
c_p(J/kgk)	2010	765
ρ (kg/m^3)	810	3970
k (Wm^{-1}K^{-1})	0.15	40
β (1/K)	9.9×10^{-4}	0.89×10^{-5}

isotropic, and homogeneous so that the matrix and the incompressible fluid of the porous medium are unchangeable. In this research, the temperature of the working fluid is the same as the solid phase temperature inside the assumed porous areas, and the notion of local thermal equilibrium (LTE) is applied. The physical features of the nanofluid remain constant regardless of the density difference, satisfying the expression of the body force by the momentum equation of Boussinesq approximation. Viscous and radiation dissipation are not considered in this research.

The equation set determining the nanofluid two-dimensional movement inside a porous medium under the subse-quent suppositions is as [8]:

Equation of continuity:

$$\frac{\partial \mathrm{u}}{\partial \mathrm{x}}+\frac{\partial \mathrm{v}}{\partial \mathrm{y}}=0 \tag{1}$$

x-momentum equation:

$$\rho_{nf}\left(\frac{1}{\varepsilon}\frac{\partial u}{\partial t}+\frac{1}{\varepsilon^2}\left(u\frac{\partial u}{\partial x}+v\frac{\partial u}{\partial y}\right)\right)=-\frac{\partial p}{\partial x}+\frac{1}{\varepsilon}\left[\left(\frac{\partial}{\partial x}\left(\mu_{nf}\frac{\partial u}{\partial x}\right)+\frac{\partial}{\partial y}\left(\mu_{nf}\frac{\partial u}{\partial y}\right)+\frac{\partial \mu_{nf}}{\partial y}\frac{\partial v}{\partial x}+\frac{\partial \mu_{nf}}{\partial x}\frac{\partial u}{\partial x}\right]-\frac{\mu_{nf}}{K}u-\frac{F_c}{\sqrt{K}}u\sqrt{u^2+v^2}\right. \tag{2}$$

y-momentum equation:

$$\rho_{nf,0}\left(\left(\frac{1}{\varepsilon}\frac{\partial v}{\partial t}+\frac{1}{\varepsilon^2}u\frac{\partial v}{\partial x}+v\frac{\partial v}{\partial y}\right)\right)=-\frac{\partial p}{\partial y}+\frac{1}{\varepsilon}\left[\frac{\partial}{\partial x}\left(\mu_{nf}\frac{\partial v}{\partial x}\right)+\frac{\partial}{\partial y}\left(\mu_{nf}\frac{\partial v}{\partial y}\right)+\frac{\partial \mu_{nf}}{\partial y}\frac{\partial v}{\partial y}+\frac{\partial \mu_{nf}}{\partial x}\frac{\partial u}{\partial y}\right]-\frac{\mu_{nf}}{K}v-\frac{F_c}{\sqrt{K}}v\sqrt{u^2+v^2}+(\rho\beta)_{nf}g(T-T_c) \tag{3}$$

Equation of energy:

$$(\rho c_p)_{nf}\left(\sigma\frac{\partial T}{\partial t}+u\frac{\partial T}{\partial x}+v\frac{\partial T}{\partial y}\right)=\frac{\partial}{\partial x}\left(k_{nf}\frac{\partial T}{\partial x}\right)+\frac{\partial}{\partial y}\left(k_{nf}\frac{\partial T}{\partial y}\right) \tag{4}$$

At reference temperature, the nanofluid effective density is:

$$\rho_{nf}=(1-\phi)\rho_f+\phi\rho_p \tag{5}$$

Nanofluid thermal expansion and specific heat capacity, which were presented by Xuan and Li [34], respectively, are:

$$(\rho\beta)_{nf}=(1-\varphi)(\rho\beta)_f+\varphi(\rho\beta)_p \tag{6}$$

$$(\rho c_p)_{nf}=(1-\varphi)(\rho c_p)_f+\varphi(\rho c_p)_p \tag{7}$$

Structural fluid thermal conductivity based on the model of Chon et al. [35] is as follows:

$$\frac{k_{nf}}{k_f}=1+64.7\varphi^{0.4076}\left(\frac{d_f}{d_p}\right)^{0.3690}\left(\frac{k_p}{k_f}\right)^{0.7476}Pr^{0.9955}Re^{1.232} \tag{8}$$

here, d_p and d_f are nanoparticle size and molecular diameter of base fluid, respectively. The particle size in this study is 47 nm. Re and Pr are defined by the following:

$$\mathrm{Re}=\frac{\rho_f k_b T}{3\pi\mu_f l_f} \tag{9}$$

$$\mathrm{Pr}=\frac{\mu_f}{\rho_f\alpha_f} \tag{10}$$

where l_f=0.17 nm and k_b=1.3807×10^{-23} J/K are the fluid particle mean path and the Boltzmann constant, respectively [35]. Angue Minsta et al.'s experiment [35] confirmed Chon et al.'s model precision. The dynamic viscosity of nanofluid μnf developed by Brinkman *et al.* [36], is stated as follows:

$$\mu_{nf} = \frac{\mu_f}{(1-\varphi)^{5/2}} \quad (11)$$

The Forcheimer coefficient (F_c) is described using the Ergun's experiential study as [36]:

$$F_c = \frac{1.75}{\sqrt{150}\varepsilon^{3/2}} \quad (12)$$

The specific heat ratio σ is assumed to be 1, taking into account the fact that the fluid and solid phases are the same [30].

$$\sigma = \frac{\varepsilon(\rho c_p)_{nf}+(1-\varepsilon)(\rho c_p)_p}{(\rho c_p)_{nf}} \quad (13)$$

By applying the dimensionless variables, they are given as:

$$X = \frac{x}{L} \quad Y = \frac{y}{L} \quad \tau = \frac{U_p t}{L} \quad U = \frac{u}{U_p}$$

$$V = \frac{v}{U_p} \quad P = \frac{p}{\rho_f U_P^2} \quad \theta = \frac{T-T_c}{T_h-T_c}$$

The governing equations in the dimensionless form are given below:

Equation of continuity:

$$\frac{\partial \mathrm{U}}{\partial \mathrm{X}} + \frac{\partial \mathrm{V}}{\partial \mathrm{Y}} = 0 \quad (14)$$

x-momentum equation:

$$\frac{1}{\varepsilon}\frac{\partial U}{\partial \tau} + \frac{1}{\varepsilon^2}\left[U\frac{\partial U}{\partial X} + V\frac{\partial U}{\partial Y}\right] = -\frac{\rho_f}{\rho_{nf}}\frac{\partial P}{\partial X} + \frac{1}{\varepsilon}\frac{1}{Re\times\upsilon_f\times\rho_{nf}}\left[\frac{\partial}{\partial X}\left(\mu_{nf}\frac{\partial U}{\partial X}\right) + \frac{\partial}{\partial Y}\left(\mu_{nf}\frac{\partial U}{\partial Y}\right) + \frac{\partial \mu_{nf}}{\partial Y}\frac{\partial V}{\partial X} + \frac{\partial \mu_{nf}}{\partial X}\frac{\partial U}{\partial X}\right] - \frac{1}{Re\times\upsilon_f\times\rho_{nf}}\frac{U}{Da} - \frac{F_c}{\sqrt{Da}}U\sqrt{(U^2+V^2)} \quad (15)$$

y-momentum equation:

$$\frac{1}{\varepsilon}\frac{\partial V}{\partial \tau} + \frac{1}{\varepsilon^2}\left[U\frac{\partial V}{\partial X} + V\frac{\partial V}{\partial Y}\right] = -\frac{\rho_f}{\rho_{nf}}\frac{\partial P}{\partial Y} + \frac{1}{Re\times\upsilon_f\times\rho_{nf}}\left[\frac{\partial}{\partial X}\left(\mu_{nf}\frac{\partial V}{\partial X}\right) + \frac{\partial}{\partial Y}\left(\mu_{nf}\frac{\partial V}{\partial Y}\right) + \frac{\partial \mu_{nf}}{\partial Y}\frac{\partial V}{\partial Y} + \frac{\partial \mu_{nf}}{\partial X}\frac{\partial U}{\partial Y}\right] - \frac{1}{Re\times\upsilon_f\times\rho_{nf}}\frac{V}{Da} - \frac{F_c}{\sqrt{Da}}V\sqrt{(U^2+V^2)} + \frac{(\rho\beta)_{nf}}{\beta_f\rho_{nf}}Ri\theta \quad (16)$$

Equation of energy:

$$\frac{\partial \theta}{\partial \tau} + U\frac{\partial \theta}{\partial X} + V\frac{\partial \theta}{\partial Y} = \frac{1}{Re\times Pr\times\alpha_f\times(\rho c_p)_{nf}}\left[\frac{\partial}{\partial X}\left(k_{nf}\frac{\partial \theta}{\partial X}\right) + \frac{\partial}{\partial Y}\left(k_{nf}\frac{\partial \theta}{\partial Y}\right)\right] \quad (17)$$

The Grashof, Richardson, Reynolds, Prandtl and Darcy numbers presented in the above equations are respectively determined as follows:

$$Gr = \frac{g\beta_f L^3(T_h-T_c)}{\nu_f^2} \qquad Ri = \frac{Gr}{Re^2}$$

$$Re = \frac{U_p L}{\upsilon_f} \qquad Pr = \frac{\nu_f}{\alpha_f} \quad Da = \frac{K}{L^2} \quad (18)$$

For the above-mentioned model, it can be described as non-dimensional boundary constraints using non-dimensional variables as follows:

For the entire geometry domain at τ = 0: θ = 0; U = V = 0,

When τ > 0

Dimensionless boundary conditions are:

On the heat source and $\mathrm{X} = 0,$

$$\mathrm{U} = \mathrm{V} = 0, \theta = 1$$

$$\mathrm{X} = 1, 0 \le \mathrm{Y} \le 1 : \mathrm{U} = \mathrm{V} = 0, \theta = 0$$

$$\mathrm{Y} = 0, 0 \le \mathrm{X} \le 1 : \mathrm{U} = \mathrm{V} = 0, \frac{\partial \theta}{\partial \mathrm{Y}} = 0$$

$$\mathrm{Y} = 1, 0 \le \mathrm{X} \le 1 : \mathrm{V} = 0, \frac{\partial \theta}{\partial \mathrm{Y}} = 0;$$

in case 1: $U = 1,$ and case 2: $U = -1,$

The calculation of the Nusselt number on the vertical hot wall is as follows:

$$Nu = \frac{-k_{nf}}{k_f} \frac{\partial \theta}{\partial X}\Big|_{X=0} \quad (20)$$

where k_{nf}/k_f is computed by Eq. (8). Ultimately, the Nu_{avg} on the hot wall is as:

$$Nu_{avg} = \int_{1/3}^{2/3} Nu(Y)dY \quad (21)$$

Using the Galerkin Weighted Residual (GWR) tech-nique of the Finite Element Method (FEM), the non-dimensional governing equations (14)-(17) together with boundary conditions (19) were solved. This method has been discussed in detail by Hoque et al. [37, 38], Zienkiewicz et al. [39], Nasrin et al. [40] and Codina [41]. The leading non-linear partial derivatives are transported to a set of integrals using the GWR method. Later, quadrature Gaussian is used to integrate all the terms of these equations. Therefore, the nonlinear algebraic equa-tions are specified and changed by boundary con-ditions. The partial derivative solver is adapted in the Newton-Raphson iteration method through the MATLAB interface to solve nonlinear algebraic equations in matrix format. The present solutions have a convergence criterion along with error cal-culation as a set of $|Im + 1 - Im| \leq 10\text{-}6$, where I and m are the dependent variable (U, V, θ, Φ) and the iteration number, respectively.

To verify the validity of the derived scientific model and the precision of the numerical outputs in the current research, it is necessary to correlate the previously reported results. However, the prediction verification against experiment was not carried out due to the absence of experimental data on the particular problems and their associated limit states that were investigated in this research. Nevertheless, comparing the existing numerical model has been done with the research of Rajaratinam *et al.* [30] are shown in Table 2. For turbulent convection in a square sliding lid enclosure comprising nanofluids, the present numerical solution in a finite volume environment was tested by Rajaratin *et al.* [30]. A physical problem including a square enclosure with a sloped lid filled with porous media was evaluated by Rajaratinam *et al.* [30]. Three scenarios of lower and upper walls movement in opposite directions, movement of the upper wall and movement of the lower and upper walls were investigated by the authors with similar methods. One of the vertical walls of the enclosure is kept at a higher temperature and the other at a lower temperature. The comparison of the Nu_{avg} (at the hot wall) between the result of the current code for different solid volume fractions for the inclination angle (γ = 0), Darcy number (Da=10-3), and Richardson number (Ri=1) and the results obtained by Rajaratinam *et al.* [30] are given in Table 2. It should be noted that a remarkable similarity was obtained between the comparative results and published studies. Obviously, the current findings are in good agreement with the results described by Rajaratinam *et al.* [30]. With this verification, the confidence in the numerical result of the present research increases.

The finite volume method based on the control volume was numerically applied to the governing equations related to the boundary conditions. The iterative solution of the coupled system of governing equations was also done by the SIMPLE algorithm. A second-order central difference and upwind scheme were used to discrete the convection terms.

A uniform grid system was used and in order to ensure the grid independency of the solutions, various grids of 31×31, 61×61, 91×91, 121×121, 151×151 and 181×181 were examined for, D=2L/3, Ri=0.1 and $\varphi = 0.06$ in the case of one. Table 3 shows Nu_{avg} values along the hot wall attained for the different grid systems used. According to the data in Table 3, the 151×151 grid system warrants a grid-independent solution.

Table 2: Comparing Nu with the cases of [30].

φ	Nu [30]	Current study
0.0	5.4	5.3
0.03	5.9	5.73
0.05	6.2	6.15

Table 3: Nu_{avg} in grid independency tests for case 1 at Ri=0.1, D=2L/3 and ϕ =0.06.

Grid size	31×31	61×61	91×91	121×121	151×151	181×181
Nu_{avg}	5.781	6.527	6.989	7.092	7.105	7.105

RESULTS AND DISCUSSION

The results have been gained for Richardson numbers between 0.01 and 100, φ between 0.0 and 0.06 and the location of the heated part, D, equal to 0, L/3 and 2L/3. The Grashof number remains constant at 10^4; hence, the Reynolds number changes as the Richardson number change.

Fig. 2 presents the isotherms and streamlines for pure water as well as the nanofluid with φ=0.06 in case I for different Richardson numbers. Streamlines show that a primary clockwise recirculation zone is formed inside the cavity. At Ri=0.01 and Ri=0.1, where forced convection plays the main role, a thermal boundary layer is formed in the vertical wall vicinity. Also as shown by the isotherms, the cavity's large core region has approximately the same temperature. Due to the coincidence of the moving lid with the fluid, a region of relative vacuum is created in the upper left corner, and then the effect of nanofluid application on the isotherms, prominent streamlines are deflected from this region. It is seen from the plots of isotherms that when forced convection is dominant. Natural convection is dominant at Ri=10 and Ri=100. The isotherms for the cases of Ri=10 and Ri=100, where conduction dominates the flow regime, show that the adsorption isotherms are vertical towards the heat source. At the lower Richardson number values, the boundary layers become more distinct and the flow strength enhances. The isotherms display that the gradient of temperature becomes steeper near the heater and the cold wall.

Isotherms and streamlines for the base fluid and nanofluid at various Richardson numbers in case II are shown in Fig. 3. In this case, the buoyancy forces to the right and the forces due to the moving wall operate in the opposite directions. For Ri=0.01, only a strong counterclockwise rotation region is formed in the cavity, but as the Richardson number increases, this counterclockwise rotation weakens, so that at Ri=10 a secondary clock wise rotation is formed which gets stronger for Ri=100.

At Ri=1, natural convection and forced convection have similar strength. To investigate the impacts of the location of the heat source, the streamlines and isotherms are illustrated in Figs. 4 and 5 for cases I and II, respectively, at Ri=1 for different heat source locations. It is observed that, for case I, regardless of the location of the heat source, only one clockwise circulation region is formed. This is because the movable lid aids the flow. In case II, a primary counterclockwise recirculation is formed at the top, and a secondary clockwise recirculation region is formed at the cavity bottom when D=2L/3 and D=0. It is because of the free space that is created at the bottom. But at D=L/3, there is not enough free space for creating secondary recirculation. It is noticed from the isotherms that the temperature field is greatly influenced by changing the heat source location.

To study the influence of Ri and φ for a constant D, the values of Nu_{avg} on the heat source are shown in Fig. 6 for various Ri and φ in cases I and II. The value of Nu_{avg} at Ri=0.01 and 0.1 is higher than Ri=10 and 100 for all volume fractions in two cases. This is because of the strong strength of forced convection at R=0.01 and 0.1 which induces heat transfer significantly. Nu_{avg} increases in both cases with increasing the volume fraction of the nanoparticle. However, free convection heat transfer is dominant at Ri=10 and 100; hence, the rate of increase is less than that of Ri=0.01 and 0.1. In case I, for every Ri and φ the value of Nu_{avg} is greater than in case II. This is due to the opposite influence of forced convection on free convection in case II.

To investigate the impact of heat source location on the values of Nu_{avg} on the heat source are shown in Fig. 7 for various volume fractions and D at Ri=1 for cases I (Fig. 7a) and II (Fig. 7b). Nu_{avg} increases in two cases by moving the heat source location from the left wall to the upper wall. It is observed that the addition of Al_2O_3 nanoparticles increases the rate of heat transfer for all of the heat source locations in case I. While using nanofluid with any volume fraction, it has no impact on Nu_{avg} when the heat source is placed in case II at D=0. In addition, the increase of Nu_{avg} for other D values is more pronounced in case I compared to case II. These are related to the effects of the direction of lid motion, which aids convection in the cavity in case I and opposes it in case II.

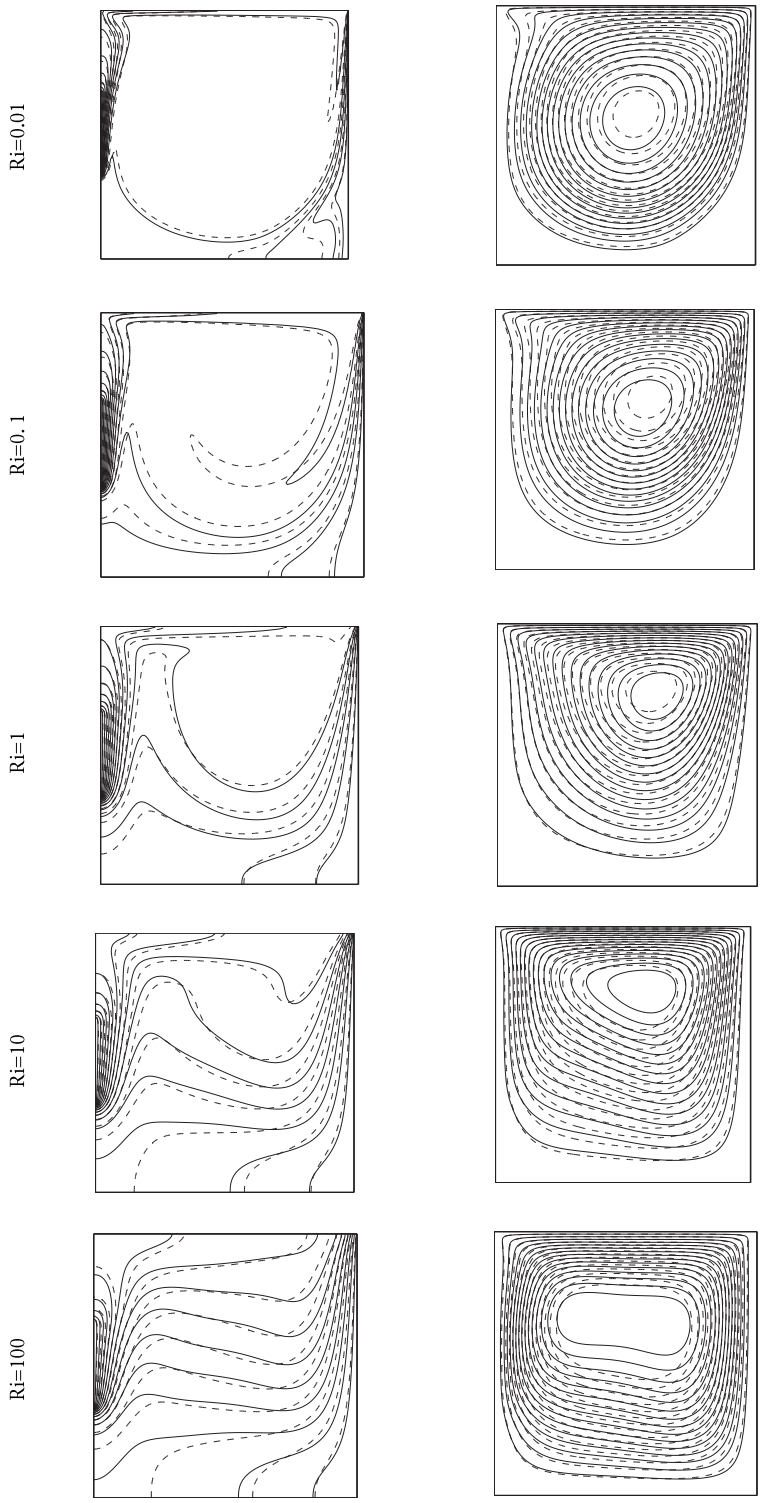

Fig. 2. Streamlines (right) and isotherms (left) for case I with various Ri and the heated portion located in D = L/3 (solid lines: pure water and dashed lines: nanofluid with φ=0.06).

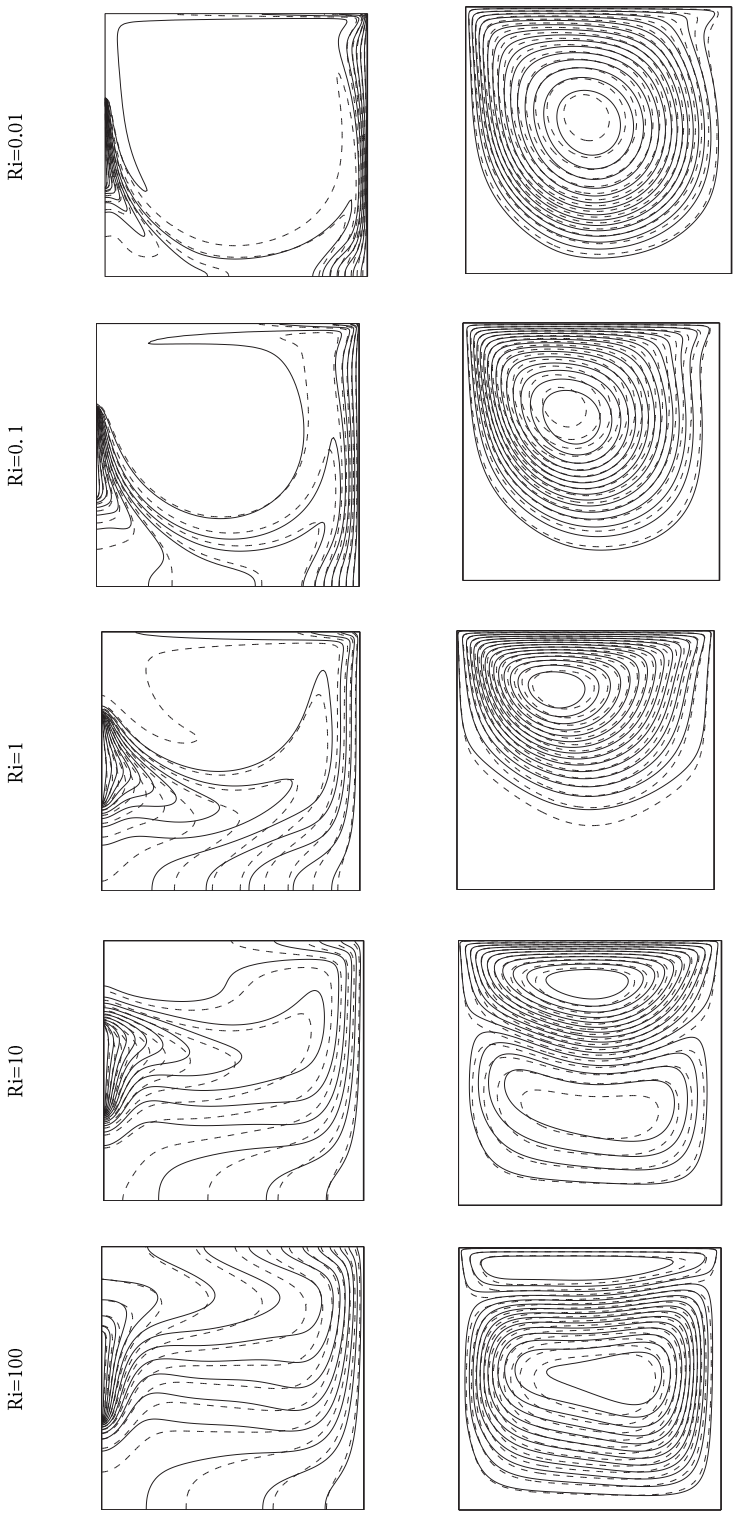

Fig. 3. Streamlines (right) and isotherms (left) for case II with various Ri and the heated portion located in D=L/3 (solid lines: pure water and dashed lines: nanofluid with φ=0.06).

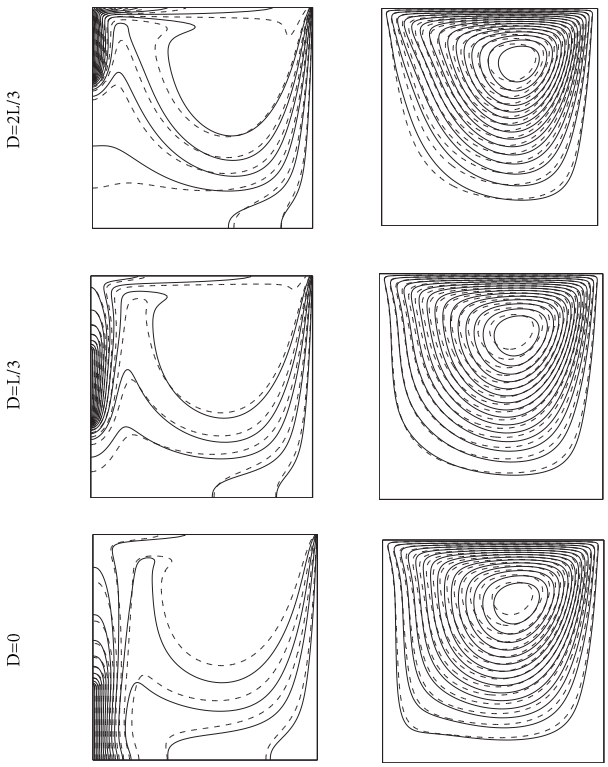

Fig. 4. Streamlines (right) and isotherms (left) for case I at Ri=1 for different locations of heat source.

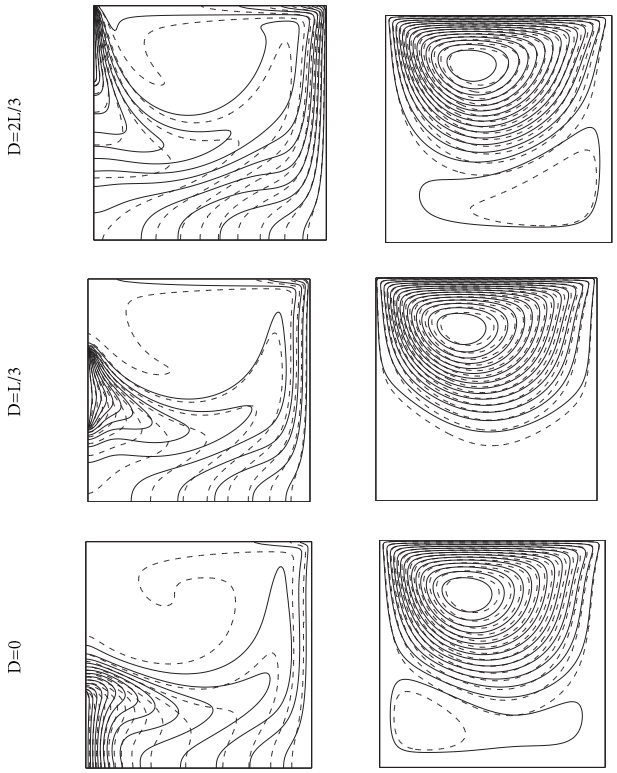

Fig. 5. Streamlines (right) and isotherms (left) for case II at Ri=1 for different locations of heat source.

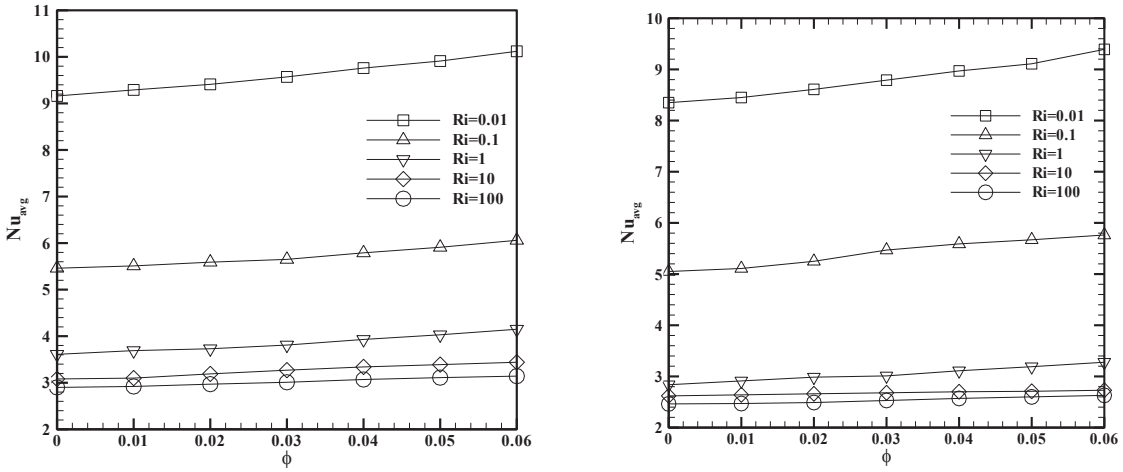

Fig. 6. Nuavg on the heat source versus volume fraction of nanoparticles for various Ri and D=L/3: (a) case I, (b) case II.

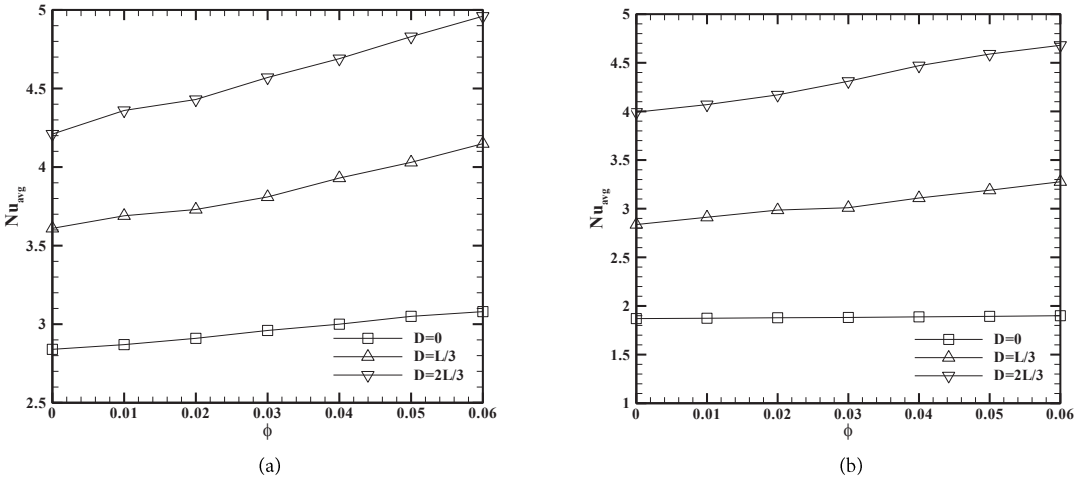

Fig. 7. Nuavg on the heat source versus volume fraction of nanoparticles for different locations of heat source and Ri=1: (a) case I, (b) case II.

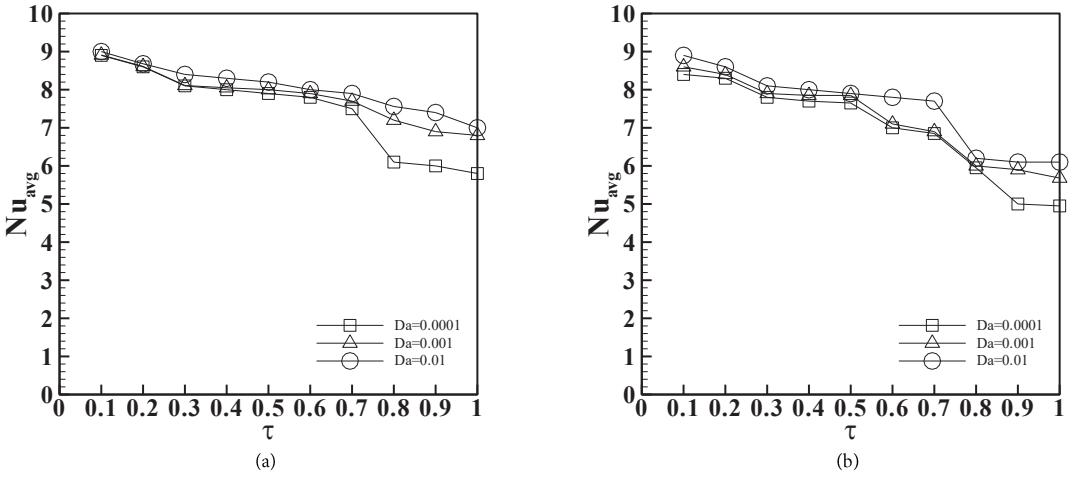

Fig. 8. Nuavg on the heat source versus τ for Darcy number: (a) case I, (b) case II.

Fig. 8 shows the changes of the average Nusselt number in terms of dimensionless time (τ) and different Darcy numbers (Da). As shown in the figure for cases I (Fig. 8a) and II (Fig. 8b), the Nusselt number increases with the increasing dimensionless time for both cases, while it is increased with the increasing of the Darcy number due to the decrease in fluid flow resistance.

CONCLUSIONS

In this article, a numerical study has been conducted to study the convection of kerosene-alumina nanofluid with variable properties in a moving lid cavity filled with different heat source locations on the hot wall for two cases of lid motion direction. The following results are obtained based on this numerical study:

1- The average Nusselt number in both cases increases with increasing nanoparticle volume fraction.
2- Forced convection is dominant at lower Ri values; hence the higher rate of heat transfer from the heat source is experienced. However, in case II, where the lid moves toward the left, the heat transfer rate is reduced due to the opposite effect of the viscous force caused by the displacement of the lid with the buoyancy force induced by the heat source.
3- Heat source displacement in case II has a different influence on Nu_{avg} compared to case I.
4- Nu_{avg} increases with increasing of τ , while it increases with increasing Da.

Nomenclature

g	Gravitational acceleration
Gr	Grashof number
H	Enclosure height
Nu	Nusselt number
k	Thermal conductivity
p	Pressure
P	Dimensionless pressure
Pr	Prandtl number
Da	Darcy number
Ra	Rayleigh number
Re	Reynolds number
Ri	Richardson number
T	Temperature
u, v	Components of velocity
U, V	Dimensionless of velocity component
Up	Velocity of the moving lid
x, y	Cartesian coordinates
X, Y	Dimensionless of Cartesian coordinates

Greek symbols

α	Thermal diffusivity
β	Thermal expansion coefficient
ϕ	Solid volume fraction
μ	Dynamic viscosity
ν	Kinematics viscosity
ρ	Density
θ	Dimensionless temperature
τ	Dimensionless time

Subscript

avg	average
c	Cold wall
eff	Effective
f	Fluid
h	Hot wall
nf	Nanofluid
p	Particle

CONFLICT OF INTEREST

THE AUTHORS DECLARE NO CONFLICTS OF INTEREST.

REFERENCES

[1] Choi S. U. S., Eastman J. A., (1995), Enhancing thermal conductivity of fluids with nanoparticles, argonne national lab., IL, No. ANL/MSD/CP-84938; CONF- 951135-29.
[2] Buongiorno J., (2006), Convective transport in nanofluids J. Heat Transf. 128: 240-250. https://doi.org/10.1115/1.2150834
[3] Kakaç S., Pramuanjaroenkij A., (2009), Review of convective heat transfer enhancement with nanofluids. Int. J. Heat Mass Transf. 52: 3187-3196. https://doi.org/10.1016/j.ijheatmasstransfer.2009.02.006
[4] Sajid M. U., Ali H. M., (2019), Recent advances in application of nanofluids in heat transfer devices: A critical review. Sustain. Energy Rev. 103: 556-592. https://doi.org/10.1016/j.rser.2018.12.057
[5] Alhajaj Z., Bayomy A. M., Saghir M. Z., (2019), A comparative study on best configuration for heat enhancement using nanofluid. Int. J. Thermofluids 7-8: 100041. https://doi.org/10.1016/j.ijft.2020.100041
[6] Manzoor A. T., Saghir M. Z., (2021), Heat transfer enhancement in multiple pipes configuration using different fluid mixtures: A numerical approach. Int. J. Thermofluids. 10: 100088. https://doi.org/10.1016/j.ijft.2021.100088
[7] Olabi A. G., Sayed E. T., Wilberforce T., Elsaid K., Rahman S. M. A., Abdelkareem M. A., (2021), Geometrical effect coupled with nanofluid on heat transfer enhancement in heat exchangers. Int. J. Thermofluids. 10: 100072. https://doi.org/10.1016/j.ijft.2021.100072
[8] Nield D. A., Bejan A., (2019), Convection in porous media, 3, Springer, New York, 2006.
[9] Zing C., Mahjoob S., Vafai K., (2019), Analysis of porous filled heat exchangers for electronic cooling. Int. J. Heat Mass Transf. 133: 268-276. https://doi.org/10.1016/j.ijheatmasstransfer.2018.12.067
[10] Xu H. J., Xing Z. B., Wang F. Q., Cheng Z. M., (2019),

Review on heat conduction, heat convection, thermal radiation and phase change heat transfer of nanofluids in porous media: Fundamentals and applications. Chem. Eng. Sci. 195: 462-483. https://doi.org/10.1016/j.ces.2018.09.045

[11] Alhajaj Z., Bayomy A. M., Ziad Saghir M., Rahman M. M., (2020), Flow of nanofluid and hybrid fluid in porous channels: Experimental and numerical approach. Int. J. Thermofluids. 1-2: 100016. https://doi.org/10.1016/j.ijft.2020.100016

[12] Sheremet M. A., Pop I., (2015), Free convection in a porous horizontal cylindrical annulus with a nanofluid using Buongiorno's model. Comput. Fluids. 118: 182-190. https://doi.org/10.1016/j.compfluid.2015.06.022

[13] Gros¸an T., Revnic C., Pop I., Ingham D.B., (2015), Free convection heat transfer in a square cavity filled with a porous medium saturated by a nanofluid. Int. J. Heat Mass Transf. 87: 36-41. https://doi.org/10.1016/j.ijheatmasstransfer.2015.03.078

[14] Yahya M., Saghir M. Z., (2021), Thermal analysis of flow in a porous flat tube in the presence of a nanofluid: Numerical approach. Int. J. Thermofluids. 10: 100095. https://doi.org/10.1016/j.ijft.2021.100095

[15] Karim M. F., Huq S., Azad A. K., Chowdhury M. S. R., Rahman M. M., (2021), Numerical analysis of thermofluids inside a porous enclosure with partially heated wall. Int. J. Thermofluids. 11: 100099. https://doi.org/10.1016/j.ijft.2021.100099

[16] Plant R. D., Saghir M. Z., (2021), Numerical and experimental investigation of high concentration aqueous alumina nanofluids in a two and three channel heat exchanger. Int. J. Thermofluids. 9: 100055. https://doi.org/10.1016/j.ijft.2020.100055

[17] Aly A. M., Raizah Z. A. S., Sheikholeslami M., (2020), Analysis of mixed convection in a sloshing porous cavity filled with a nanofluid using ISPH method. J. Therm. Anal. Calorimetry. 139: 1977-1991. https://doi.org/10.1007/s10973-019-08575-0

[18] Izadi M., Mohebbi R., Delouei A. A., Sajjadi H., (2019), Natural convection of a magnetizable hybrid nanofluid inside a porous enclosure subjected to two variable magnetic fields. Int. J. Mech. Sci. 151: 154-169. https://doi.org/10.1016/j.ijmecsci.2018.11.019

[19] Sheikholeslami M., (2019), Numerical approach for MHD Al2O3-water nanofluid transportation inside a permeable medium using innovative computer method. Comput. Methods Appl. Mech. Eng. 344: 306-318. https://doi.org/10.1016/j.cma.2018.09.042

[20] Sheikholeslami M., Ziabakhsh Z., Ganji D. D., (2017), Transport of magnetohydrodynamic nanofluid in a porous media. Colloids and Surf. A: Physicochem. Eng. Aspects. 520: 201-212. https://doi.org/10.1016/j.colsurfa.2017.01.066

[21] Sheikholeslami M., Shehzad S. A., (2018), CVFEM simulation for nanofluid migration in a porous medium using darcy model. Int. J. Heat Mass Transf. 122: 1264-1271. https://doi.org/10.1016/j.ijheatmasstransfer.2018.02.080

[22] Xu H., Gong L., Huang S., Xu M., (2015), Flow and heat transfer characteristics of nanofluid flowing through metal foams. Int. J. Heat Mass Transf. 83: 399-407. https://doi.org/10.1016/j.ijheatmasstransfer.2014.12.024

[23] Al-Weheibi S. M., Rahman M. M., Saghir M. Z., (2020), Impacts of variable porosity and variable permeability on the thermal augmentation of Cu-H2O Nanofluid-drenched porous trapezoidal enclosure considering thermal nonequilibrium model. Arab. J. Sci. Eng. 45: 1237-1251. https://doi.org/10.1007/s13369-019-04234-6

[24] Kalbani Al., Khamis S., Rahman M. M., Ziad Saghir M., (2020), Entropy generation in hydromagnetic nanofluids flow inside a tilted square enclosure under local thermal nonequilibrium condition. Int. J. Thermofluids. 5: 100031. https://doi.org/10.1016/j.ijft.2020.100031

[25] Hussain S., Mehmood K., Sagheer M., Farooq A., (2017), Entropy generation analysis of mixed convective flow in an inclined channel with cavity with Al2O3-water nanofluid in porousmedium.Int.Commun.HeatMassTransf.89:198-210. https://doi.org/10.1016/j.icheatmasstransfer.2017.10.009

[26]CimpeanD.S.,PopI.,(2012),Fullydevelopedmixedconvection flow of a nanofluid through an inclined channel filled with a porous medium. Int. J. Heat Mass Transf. 55: 907-914. https://doi.org/10.1016/j.ijheatmasstransfer.2011.10.018

[27] Al-Rashed A. A., Sheikhzadeh G. A., Aghaei A., Monfared F., Shahsavar A., Afrand M., (2020), Effect of a porous medium on flow and mixed convection heat transfer of nanofluids with variable properties in a trapezoidal enclosure. J. Therm. Anal.Calorimetry. 139: 741-754. https://doi.org/10.1007/s10973-019-08404-4

[28] Tahmasbi M., Siavashi M., Abbasi H. R., Akhlaghi M., (2020), Mixed convection enhancement by using optimized porous media and nanofluid in a cavity with two rotating cylinders. J. Therm. Anal. Calorimetry. 141: 1829-1846. https://doi.org/10.1007/s10973-020-09604-z

[29] Selimefendigil F., Chamkha A. J., (2021), MHD mixed convection of Ag-MgO/water nanofluid in a triangular shape partitioned lid-driven square cavity involving a porous compound. J. Therm. Anal. Calorimetry. 143: 1467-1484. https://doi.org/10.1007/s10973-020-09472-7

[30] Rajarathinam M., Nithyadevi N., Chamkha A. J., (2018), Heat transfer enhancement of mixed convection in an inclined porous cavity using Cu-water nanofluid. Adv. Powder Technol. 29: 590-605. https://doi.org/10.1016/j.apt.2017.11.032

[31] Ahmed S. E., Aly A. M., (2020), Mixed convection in a nanofluid-filled sloshing porous cavity including inner heated rose. J. Therm. Anal. Calorimetry. 143: 1-17. https://doi.org/10.1007/s10973-019-09216-2

[32] Astanina M. S., Sheremet M. A., Oztop H. F., Abu-Hamdeh N., (2018), Mixed convection of Al2O3-water nanofluid in a lid-driven cavity having two porous layers. Int. J. Heat Mass Transf. 118: 527-537. https://doi.org/10.1016/j.ijheatmasstransfer.2017.11.018

[33] Mahmoodi M., Kandelousi S., (2016), Cooling process of liquid propellant rocket by means of kerosene-alumina nanofluid. Propulsion and Power Res. 5: 279-286. https://doi.org/10.1016/j.jppr.2016.11.003

[34] Xuan Y., Li Q., (2003), Investigation on convective heat transfer and flow features of nanofluids. ASME J. Heat Trans. 125: 151-155. https://doi.org/10.1115/1.1532008

[35] Chon C. H., Kihm K. D., Lee S. P., Choi S. U. S., (2005), Empirical correlation finding the role of temperature and particle size for nanofluid (Al2O3) thermal conductivity enhancement. Appl. Phys. Lett. 87: 103-107. https://doi.org/10.1063/1.2093936

[36] Brinkman H. C., (1952), The viscosity of concentrated suspensions and solutions. J. Chem. Phys. 20: 571-578.

https://doi.org/10.1063/1.1700493
[36] Ergun S., (1952), Fluid flow through packed columns. Chem. Eng. Prog. 48: 89-94.
[37] Hoque K. E., Ferdows M., Sawall S., Tzirtzilakis E. E., Xenos M. A., (2021), Hemodynamic characteristics expose the atherosclerotic severity in coronary main arteries: One dimensional and three-dimensional approaches. Phys. Fluids. 33: 121907. https://doi.org/10.1063/5.0069106
[38] Hoque K. E., Ferdows M., Sawall S., Tzirtzilakis E. E., Xenos M. A., (2021), The impact of hemodynamic factors in a coronary main artery to detect the atherosclerotic severity: Single and multiple sequential stenosis cases. Phys. Fluids. 33: 031903. https://doi.org/10.1063/5.0041335
[39] Nasrin R., Saddam H., Zahan I., Ahmed K. F. U., Fayaz H., (2020), Performance analysis of hybrid nanofluid on enhancement of fluid thermal conductivity in liddriven undulated cavity. Heat Transf. J. 49: 4204-4225. https://doi.org/10.1002/htj.21823
[40] Zienkiewicz O. C., Taylor R. L., Zhu J. Z., (2005), The finite element method: Its basis and fundamentals. Elsevier Book.
[41] Codina R., (1998), Comparison of some finite element methods for solving the diffusion convection-reaction equation. Comput. Methods in Appl. Mech. Eng. 156: 185-210. https://doi.org/10.1016/S0045-7825(97)00206-5